Computer-aided detection and quantification of endolymphatic hydrops within the mouse cochlea *in vivo* using optical coherence tomography

George S. Liu
Jinkyung Kim
Brian E. Applegate
John S. Oghalai

SPIE.

Computer-aided detection and quantification of endolymphatic hydrops within the mouse cochlea *in vivo* using optical coherence tomography

George S. Liu,[a] **Jinkyung Kim,**[a] **Brian E. Applegate,**[b] **and John S. Oghalai**[a,*]
[a]Stanford University, Department of Otolaryngology–Head and Neck Surgery, Stanford, California, United States
[b]Texas A&M University, Department of Biomedical Engineering, College Station, Texas, United States

Abstract. Diseases that cause hearing loss and/or vertigo in humans such as Meniere's disease are often studied using animal models. The volume of endolymph within the inner ear varies with these diseases. Here, we used a mouse model of increased endolymph volume, endolymphatic hydrops, to develop a computer-aided objective approach to measure endolymph volume from images collected *in vivo* using optical coherence tomography. The displacement of Reissner's membrane from its normal position was measured in cochlear cross sections. We validated our computer-aided measurements with manual measurements and with trained observer labels. This approach allows for computer-aided detection of endolymphatic hydrops in mice, with test performance showing sensitivity of 91% and specificity of 87% using a running average of five measurements. These findings indicate that this approach is accurate and reliable for classifying endolymphatic hydrops and quantifying endolymph volume. © *2017 Society of Photo-Optical Instrumentation Engineers (SPIE)* [DOI: 10.1117/1.JBO.22.7.076002]

1 Introduction

Optical coherence tomography (OCT) has been developed for minimally and noninvasive diagnostic imaging in a variety of organs, including the eye,[1–3] coronary arteries,[4] bronchi,[5] esophagus,[6] and skin.[7] More recently, there has been growing interest in using OCT to study the auditory portion of the inner ear, the cochlea (Fig. 1), in animal models.[8–13] There are many diseases that cause hearing loss and/or vertigo in patients that cannot be comprehensively studied in living humans because the inner ear is too small to be effectively imaged, and invasive tissue biopsies would lead to complete loss of hearing. However, OCT permits the noninvasive imaging of inner ear anatomy in animal models of these diseases. This approach may be particularly valuable in the study of Meniere's disease, a syndrome of episodic vertigo, fluctuating hearing loss, roaring tinnitus, and aural pressure, because it is associated with a specific histological finding called endolymphatic hydrops.[14]

Endolymphatic hydrops is the abnormal accumulation of fluid within the scala media, a compartment inside the cochlea [SM in Figs. 1(b) and 1(c)]. The etiology of endolymphatic hydrops remains poorly understood.[15] Morphologically, it is characterized by a distension of Reissner's membrane,[16] the membrane that separates scala media from scala vestibuli. In humans, it has been measured using MRI[17,18] after intratympanic injection of contrast but is typically only measured postmortem using fixed, sectioned tissue.[16] We have recently measured endolymphatic hydrops in a mouse model of blast injury by directly observing the distension of Reissner's membrane in cross-sectional OCT[19] [Fig. 1(d)] images. Subjectively, it is relatively easy for a cochlear histopathologist to say whether

endolymphatic hydrops is present simply by visualizing the distension of Reissner's membrane. Objectively, however, establishing the presence or absence of endolymphatic hydrops and quantifying the volume of endolymph are not straightforward tasks. The common approach is to assess the degree of distension of Reissner's membrane as a proxy for endolymph volume measurement.[15] This has been done in single cross sections using two different techniques: (1) by manual measurement of the ratio of the scala media area to the scala vestibuli area [SV in Figs. 1(b) and 1(c)][20] and (2) by manual measurement of the area of the scala media between Reissner's membrane and its ideal position, a line between its attachment points at the spiral limbus and the lateral wall [orange dotted line in Fig. 1(d)].[21–24]

Here, we report a computer-aided method to measure the displacement of Reissner's membrane using the second approach. We developed this specifically to classify endolymphatic hydrops in mice undergoing cochlear imaging using OCT. We show that this technique provides accurate and reliable classification of endolymphatic hydrops noninvasively. Thus, this approach permits a semiautomated and objective assessment of whether a mouse has endolymphatic hydrops as well as quantification of its severity. We expect it will facilitate research in animal models of inner ear pathologies, such as traumatic noise exposure or genetic mouse models of endolymphatic hydrops.[25]

2 Materials and Methods

2.1 Data Collection

We imaged cochleae in live mice using OCT, as described previously.[10,26] Briefly, mice were anesthetized with ketamine/ xylazine, fixed to a head post to reduce motion artifacts during

*Address all correspondence to: John S. Oghalai, E-mail: joghalai@stanford .edu
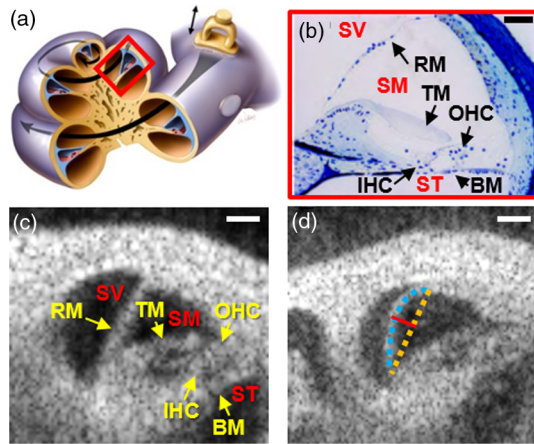
Fig. 1 Endolymphatic hydrops. (a) Schematic of the cochlea. (b) Plastic-embedded section of the upper basal turn of a mouse cochlea (adapted from Ref. 27), scale bar is 50 μm. (c) Representative OCT cross-sectional image of the same cochlear position in a mouse with a normal endolymph volume. Note that Reissner's membrane is straight. Scale bar is 100 μm. (d) Representative OCT cross-sectional image of the cochlea in a mouse with endolymphatic hydrops caused by blast exposure. Note that Reissner's membrane is bowed outward (blue dotted line). The perpendicular displacement of Reissner's membrane (red line) is measured orthogonally from the midpoint of the chord between its points of attachment at the spiral limbus and the lateral wall (orange dotted line). Scale bar is 100 μm. BM, basilar membrane; IHC, inner hair cell region; OHC, outer hair cell region; RM, Reissner's membrane; SM, scala media; ST, scala tympani; SV, scala vestibuli; and TM, tectorial membrane.

image acquisition, and underwent surgery to open the left middle ear bulla. We then imaged the cochlea without violating the otic capsule bone that surrounds it. All protocols were approved by the Institutional Animal Care and Use Committee at Stanford University.

Over the course of these experiments, we imaged the cochleae of 16 normal CBA/CaJ mice. To evaluate the effectiveness of our technique in classifying endolymphatic hydrops, five mice were exposed to a single blast pressure wave with a peak pressure of 130 kPa and four mice were exposed to band-passed white noise (8 to 16 kHz) at 100-dB sound pressure level for 2 h using previously described techniques.[27–29] We have found that mice develop endolymphatic hydrops after blast or noise exposure[19] under these conditions. (A separate paper detailing the biological features of this phenomenon is currently in preparation.) The other seven mice served as the control group and received no blast or noise exposure.

We imaged each cochlea from multiple positions and depths at a fixed angle to capture hundreds of cross-sectional images per cochlea. The angle and depths of imaging were chosen to image the midmodiolar section of the cochlea [as in Figs. 1(b)–1(d)]. The purpose of this was to keep the angle of incidence consistent across experiments for visualizing Reissner's membrane deformation. In three mice, some of the images were obtained using laser angle adjustments between 15 and −15 deg from the midmodiolar plane to evaluate the influence of angle perturbations on displacement measurements. We found similar displacement measurements in images with and without angle adjustments, and included all data in our analysis. Our results were similar with and without inclusion of images at adjusted angles. In each frame, we focused our analysis on an 80×90 pixel rectangle containing the apical turn of the

cochlea, obtained by manually cropping the raw image. The optical resolution of the imaging system was 9.8 μm lateral and 15 μm axial measured in air.[10] The higher refractive index in the cochlea (perilymph, 1.34)[30] improves the axial resolution; however, tissue-induced aberration and dispersion degrade the image quality. The sampling in the acquired images was 7.5×7.5 μm with interpolation done to obtain the correct aspect ratio.

In 10 mice, we also collected volumetric images along a 150-μm length of basilar membrane inside the cochlea. We acquired 20 cross-sectional images at intervals of 7.5 μm and stacked the images to reconstruct a three-dimensional (3-D) image of the cochlea. These data were then used to quantify endolymph volume, since this is truly a direct indicator of the severity of endolymphatic hydrops.

2.2 Ground-Truth Labeling of Images

Ground-truth labels of endolymphatic hydrops were determined visually by a trained observer (J.K.) without blinding during image acquisition and later reviewed by a second observer (G.S.L.) during image preparation. In all mice, multiple cross sections were obtained in the same cochlea, and the entire set of cross sections were viewed together to determine the ground-truth label of the cochlea and its cross sections. Of the 6391 images assessed, 3062 images were labeled as nonhydrops (controls) and 3329 images were labeled as endolymphatic hydrops. Images labeled as endolymphatic hydrops were obtained in blast- and noise-exposed mice, and images labeled as nonhydrops were obtained in control mice, with no ambiguous cases identified by the observers.

2.3 Manual Measurement of Endolymph Volume

The scala media was manually segmented in each cross section of a volumetric image. The sum of the areas of the segmented regions was then multiplied by the interval distance between adjacent cross sections (7.5 μm) to calculate the endolymph volume. Manual segmentation was performed using Amira 5.4 software (Visage Imaging, San Diego, California).

2.4 Binary Classification of Endolymphatic Hydrops Using Endolymph Volume

Prediction of endolymphatic hydrops from manually measured endolymph volume was performed using the binary classifier model

$$h_\theta(V) = \begin{cases} 1 & \text{if } V \geq \varphi, \\ 0 & \text{if } V < \varphi, \end{cases} \tag{1}$$

where V is the endolymph volume, $h_\theta(V) \in \{0,1\}$ is the prediction of endolymphatic hydrops given input V (1 = hydrops and 0 = no hydrops), and φ is the diagnostic cutoff. The diagnostic cutoff was set by training the model, using the endolymph volume data as the training dataset. Training was performed using a classification tree with one node and Gini's diversity index as the split criterion. This was done in MATLAB® using the built-in Statistics and Machine Learning Toolbox.

2.5 Manual Measurement of Reissner's Membrane Displacement

We assessed the distension of Reissner's membrane by measuring the displacement of the membrane's midpoint from its

normal position, defined as a straight line between the attachment points of Reissner's membrane at the spiral limbus medially and the spiral ligament laterally [Fig. 1(d)]. We refer to this metric as the perpendicular displacement of Reissner's membrane, and to the attachment points of Reissner's membrane as its endpoints. The sign of the displacement is positive if Reissner's membrane bows away from the scala media (increased endolymph volume, i.e., endolymphatic hydrops) and negative if it bows toward the scala media (decreased endolymph volume).

Manual segmentation was considered the gold standard for measuring the perpendicular displacement of Reissner's membrane. Manual segmentation was performed using the freehand drawing tool in the MATLAB® Image Processing Toolbox (The Mathworks, Natick, Massachusetts). With this tool, Reissner's membrane was interactively traced on the displayed image of the cochlea. The first, middle, and last points of the tracing were used to estimate the normal midpoint of Reissner's membrane and calculate its perpendicular displacement as described.

2.6 Computer-Aided Detection of Endolymphatic Hydrops

Our method of computer-aided detection involves three steps: (1) manual localization of the scala media of the apical cochlear turn in the original, uncropped OCT image, (2) automated measurement of Reissner's membrane displacement using the cropped scala media, and (3) automated prediction of endolymphatic hydrops by binary classification, using displacement as the predictor variable. Thus, the entire process should be considered semiautomated.

### 2.6.1 Manual localization of apical cochlear turn

Our method classifies OCT images in which the scala media occupies most of the image center and is oriented as shown in Figs. 1(c) and 1(d). To obtain images that meet these constraints, we acquired images in the preferred orientation during experiments and manually localized the scala media afterward. For manual localization, the user selected a point in the center of the scala media of the apical turn in the original, uncropped image using the computer mouse (Fig. 2, red asterisk). The image was then cropped to an 80×90 pixel rectangle centered on the selected point. Beyond this step, the workflow for classification was fully automated.

2.6.2 Automated measurement of Reissner's membrane displacement

Our approach to automated measurement of Reissner's membrane displacement relies on segmentation of Reissner's membrane. All codes were written in MATLAB®. Segmentation of Reissner's membrane was performed as follows (Fig. 2):

1. Morphological erosion and grayscale reconstruction[31] with a disk of radius 3 pixels were performed to smooth the image.

2. Binarization using Otsu's method[32] was used to generate a mask of fluid-filled compartments, including the scala media and scala vestibuli. These compartments exhibit low optical scattering relative to the surrounding bony labyrinth and membranes. Next, small connected components in the mask containing fewer than 200 pixels were removed to erase artifacts from noise.

3. Removal of connected components at the mask borders (i.e., containing pixels in the first or last row of the mask) was performed to create a mask of only the scala media with or without the scala vestibuli. These
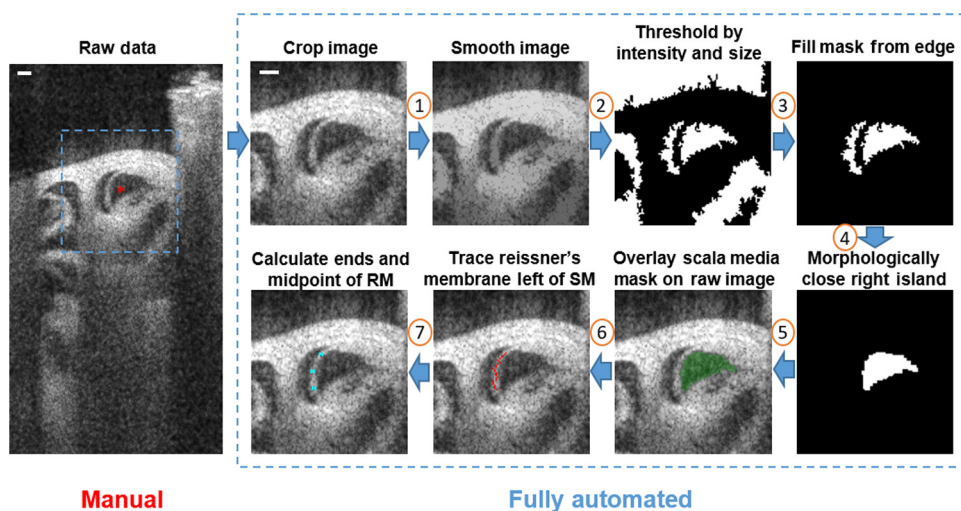
Fig. 2 Automated workflow for assessing endolymphatic hydrops. For illustration, the raw image of a mouse cochlear cross section (left) is analyzed step-by-step. The first step, cropping, requires the user to click inside the scala media (red asterisk) in the raw image. A rectangular region is then cropped (dashed blue box). Here, the cropped dimensions are 111 pixels wide × 116 pixels high. The rest of the analysis is fully automated. The cropped image is segmented from the background. The mask of the scala media (green shaded area) is overlaid on the original cropped image to segment Reissner's membrane (red line). Three points are identified on Reissner's membrane (blue asterisks) to calculate the RM perpendicular displacement. Numbered steps are explained in the text. Scale bars are 100 μm. SM, scala media and RM, Reissner's membrane.

compartments were centered in the mask because of the manual localization of the scala media.

a. As a checkpoint, the number of connected components in the mask at this point was checked. If the number was one or two, the program proceeded to step 4. Otherwise, steps 1 to 3 were repeated using an adjusted intensity threshold level in step 2. The adjusted threshold level started at Otsu's level plus 0.2 (after normalization of pixel intensities to the range [0, 1]) and iteratively decreased by 0.01 to Otsu's level minus 0.2. If none of these threshold levels resulted in a mask that satisfied this checkpoint, the program was aborted and returned "not a number (NaN)" as the displacement.

4. Morphological dilation, filling, and erosion with a 3×3 square were performed on the mask to fill spurious holes in the scala media's edges. If the mask contained two connected components, the smaller component (usually the scala vestibuli) was removed before performing this step. The mask contains only the scala media at this point.

5. The scala media mask was overlaid on the original image (Fig. 2, green shaded area).

6. Reissner's membrane was segmented using the left border of the scala media. The left border was segmented by identifying the pixel at the left end of each row of pixels in the mask. Reissner's membrane was then segmented by identifying the brightest pixel in the image among the seven pixels immediately to the left of each border pixel (Fig. 2, red line).

a. Continuity of the segmentation was checked. If the horizontal position of a segmented pixel differed from that of the pixel in the row above it by more than 15 pixels (112.5 μm), then the pixel with the deviation and all pixels below it were removed from the segmentation. This case could arise if the lower half of the segmentation of Reissner's membrane included the spiral limbus where the tectorial membrane attached, resulting in a discontinuous jump between the lower endpoint of Reissner's membrane and the spiral limbus.

b. The segmentation was smoothed. Segmented pixels with horizontal deviations were replaced with the interpolated pixels halfway between the segmented pixels in the row above and below. Horizontal position deviations were identified as differences between the pixel horizontal position and mean horizontal position of pixels in the segmentation by more than two standard deviations.

7. The midpoint and endpoints of Reissner's membrane were identified. The midpoint was estimated using the average coordinates of the four pixels in the middle rows of the segmentation. Endpoints were calculated using the average coordinates of the last four pixels at each end of the segmentation.

The end- and midpoints of Reissner's membrane were then used to calculate the displacement of Reissner's membrane. The displacement was used for binary classification of the image.

2.6.3 *Binary classification of endolymphatic hydrops using membrane displacement*

Prediction of endolymphatic hydrops from Reissner's membrane displacement was performed using the binary classifier model

$$h_\theta(D) = \begin{cases} 1 & \text{if } D \geq \theta \\ 0 & \text{if } D < \theta \end{cases}, \tag{2}$$

where D is the Reissner's membrane displacement, $h_\theta(D) \in \{0,1\}$ is the prediction of endolymphatic hydrops given input D (1 = hydrops and 0 = no hydrops), and θ is the diagnostic cutoff. The diagnostic cutoff was determined by training the model on training data.

To develop our classifier, we split our dataset of 6391 cross-sectional images from 16 mice into a training and a test dataset. The training dataset contained 5287 images from 13 mice. The test dataset contained 1104 images from three mice. A validation dataset was not needed because our classification approach only had one parameter; thus, the model cannot overfit the training data.

The model was trained using Youden's index[33] as the objective function. This identifies the diagnostic cutoff that maximizes the sum of sensitivity and specificity for training data classification. Training was performed using custom MATLAB® code. After training, the final model was evaluated on the test dataset to evaluate the model's classification performance on previously unseen images from previously unused mice. The test dataset was used only once for evaluation of the final, trained model.

2.7 *Averaging Measurements*

Information from multiple images of the same cochlea can be combined to improve the accuracy of displacement measurements. To accomplish this, we calculated the running average of measurements from five images. This was done by averaging the measurement in each image with the measurements from its four preceding images. Averaged measurements were not calculated for the first four images in each experiment. Information from multiple images included spatially adjacent cross sections from a volume image of the cochlea and temporally adjacent cross sections recorded at the same position during small adjustments to imaging position and depth of focus.

2.8 *Statistical Analysis*

Statistics were performed in MATLAB®. p values were calculated using the unpaired student's t-test. A critical alpha level of 0.05 was used to consider statistical significance. The Pearson's correlation coefficient R^2 was calculated to assess the goodness of fit of linear regressions. Data points displayed as outliers were included in all analyses.

3 Results

3.1 Displacement of Reissner's Membrane is Associated with Endolymphatic Hydrops Severity

First, we wanted to validate that the manual measurements of endolymph volume correlated with ground-truth labels as determined by two trained observers. Volumetric scans were collected from five control mice and five blast-exposed mice. Since endolymph volume changes dynamically after blast exposure, we serially repeated the scans three times in each mouse at 1-h intervals, thus collecting 30 volumetric scans in total. We then manually measured endolymph volume in each scan and correlated the measurements with the observer labels [Fig. 3(a)]. Based on these data, we trained a binary classifier, using a classification tree approach, and determined an endolymph volume threshold of 8.945 nL/150 μm to distinguish hydrops and non-hydrops. Using this threshold, these data were found to have a strong correlation ($p < 0.001$, chi-square test) with the classification by trained observers, our accepted gold standard. The sensitivity and specificity of classification were 100%, demonstrating separation of hydrops and nonhydrops measurements at this threshold.

Next, we examined whether displacement of Reissner's membrane measured from a cross-sectional image reflects the endolymph volume. We manually measured the perpendicular displacement of Reissner's membrane in cross-sectional OCT images in the same 10 mice as above. A total of 308 cross-sectional images in control mice and 307 images in blast-exposed mice were analyzed, or an average of 20.5 cross-sectional images per volume scans. We observed a larger displacement of Reissner's membrane in blast-exposed mice at all three time points compared with in control mice (34.12 ± 11.45 versus 5.26 ± 4.73 μm, mean $\pm$ SD; unpaired t-test, $p < 0.001$) [Fig. 3(b)]. Based on our data, the linear regression for endolymph volume as a function of Reissner's membrane displacement was

$$V = 7.91 + 0.0702 \times D \qquad R^2 = 0.89, \qquad (3)$$

where V is the scala media volume (in nL) over a length of 150-μm basilar membrane and D is the Reissner's membrane

displacement (in μm) [Fig. 3(b)]. This direct relationship supports an association between the displacement of Reissner's membrane and the endolymph volume. Furthermore, combining Eq. (2) and the endolymph volume threshold suggests a threshold of 14.7 μm for classifying endolymphatic hydrops using manually measured displacement. At this threshold, classification shows a strong correlation with the classification by trained observers ($p < 0.001$, chi-square test) and demonstrates sensitivity and specificity of 2.7%. These results indicate that the measured displacement is nearly as reliable as the endolymph volume for detecting endolymphatic hydrops. The next goal was to automate this process.

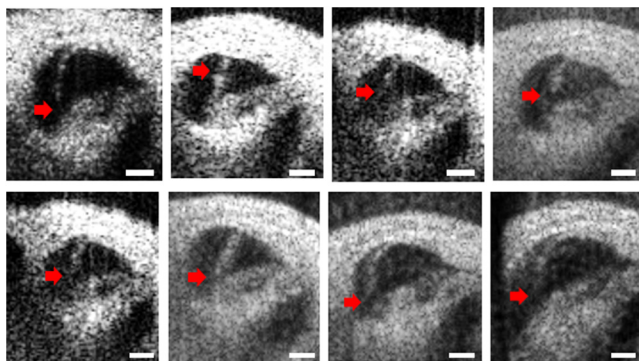## 3.2 Robustness of Automated Segmentation of Reissner's Membrane

The automated method for measuring Reissner's membrane displacement relies on segmentation of Reissner's membrane. The method returns a measurement of Reissner's membrane displacement, if it successfully segments Reissner's membrane, and returns no measurement (i.e., "NaN") otherwise. Automated analysis could be performed correctly in every mouse. However, not all OCT images were analyzable.

Our dataset of 6391 images was split into a training dataset of 5287 training images from 13 mice (including the 10 mice described above; six control mice and seven blast- or noise-exposed mice) and test dataset of 1104 images from three mice (one control and two noise exposed) for developing the binary classifier for computer-aided detection of endolymphatic hydrops. We found that 2665 of the 5287 training images (50.4%) and 958 of the 1104 test images (86.8%) could be analyzed by the method. The variation in the percentage of analyzable images between the training and test datasets suggests that the image quality, which can vary for different experiments, is important for analyzability.

In particular, we found that the appearance of Reissner's membrane as a continuous structure is important. The software often had difficulty analyzing images in which Reissner's membrane appeared to have gaps (Fig. 4, red arrows). This would result in the scala media and scala vestibuli being segmented together as one connected component, which would prevent segmentation of the scala media's left border and Reissner's
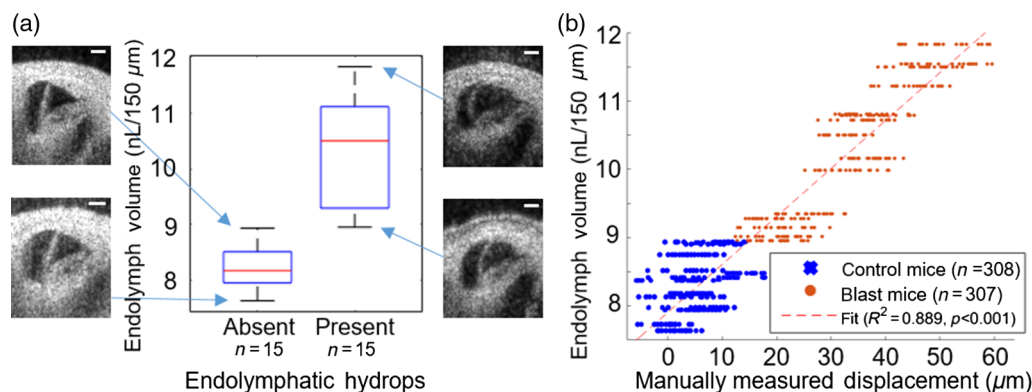
Fig. 3 Manual measurement of endolymph volume and Reissner's membrane displacement. (a) Box plot of manually measured endolymph volume along a 150-μm length of basilar membrane of cochlea using volumtric OCT, categorized by the presence or absence of endolymphatic hydrops as defined by the agreement of two trained observers viewing single cross sections. Examples of the maximum and minimum volume measurements in each exposure group are depicted. Scale bars are 100 μm. (b) Scatter plot of manually measured displacement of Reissner's membrane versus manually measured endolymph volume in the same 10 mice. The linear regression is shown as the red dashed line.

Fig. 4 Representative cross-sectional images of cochleae for which automated segmentation of Reissner's membrane could not be performed. There is a hole-like discontinuity in Reissner's membrane in the images (red arrows). The discontinuity makes it difficult to separate the scala media and scala vestibuli during thresholding, which is necessary for successful segmentation of Reissner's membrane. For these images, the automated method returns no measurement of Reissner's membrane displacement. Scale bars are 100 μm.

membrane. Thus, this approach to the automated segmentation of Reissner's membrane may not work for any single given image in isolation. However, since OCT images are acquired as a continuous stream during an experiment, this method will work if at least some of the images are clear enough to permit automated analysis.

3.3 Automated Measurement of Reissner's Membrane Displacement

To verify if automated measurements can replicate manual measurements of Reissner's membrane displacement, we performed automated measurements in the same 10 mice for which manual measurements were obtained. We compared automated and manual measurements using 30 representative cross-sectional images, one image per mouse per time point. We observed a direct association between automated and manual measurements of Reissner's membrane displacement (Pearson's correlation coefficient: $R^2 = 0.87$, $p < 0.001$) [Fig. 5(a)]. The best-fit linear regression was

$$D_m = 2.64 + 1.17 \times D_a \qquad R^2 = 0.87, \qquad (4)$$

where D_m is the manually measured Reissner's membrane displacement (in μm) and D_a is the automatically measured Reissner's membrane displacement (in μm). Though close to the identity line, the linear regression suggests that automated measurements tend to underpredict manual measurements at higher values of displacement. Overall, however, these results suggest that automated measurements of the displacement of Reissner's membrane can accurately reproduce manual measurements after applying Eq. (3) as a calibration.

We then compared the automatically measured displacements to the ground-truth labels of the trained observers. As expected, the displacement was higher in images of cochlea with endolymphatic hydrops versus without endolymphatic hydrops (15.77 ± 10.2 versus 2.12 ± 7.3 μm, mean $\pm$ SD; unpaired t-test, $p < 0.001$) [Fig. 5(b), left two columns]. To reduce the variability in the displacement data, we created a running average of the displacement from five sequential images. This approach maintained a similar difference in Reissner's

membrane displacement between the presence and absence of endolymphatic hydrops but reduced the SD (15.65 ± 6.9 versus 2.11 ± 5.3 μm, mean $\pm$ SD; unpaired t-test, $p < 0.001$) [Fig. 5(b), right two columns]. For example, in Fig. 5(d), the automatically measured displacement of Reissner's membrane in the last image (on the farthest right) was 1.7 μm without averaging and 12.3 μm with averaging, closer to the values measured in other cross sections. These data demonstrate that computer-aided classification can reliably identify endolymphatic hydrops when spatial averaging is used to improve the precision of the measurement. The necessary spatial averaging is readily achieved since OCT images are collected continuously during our experiments; hence, there is always a stream of images to work with in real time.

### 3.4 Computer-Aided Classification of Endolymphatic Hydrops

We next developed a binary classifier that uses computer-aided detection of Reissner's membrane to measure membrane displacement and predict endolymphatic hydrops status. To train the binary classifier, we performed supervised learning on 3205 computer-aided measurements of displacement and their associated ground-truth labels obtained from images in the training dataset. These data represent 2149 cross-sectional OCT images of cochlea without endolymphatic hydrops and 1056 images of cochlea with endolymphatic hydrops, and included all analyzable images in the training dataset.

We classified endolymphatic hydrops using the binary classifier model

$$h_\theta(D) = \begin{cases} 1 & \text{if } D \geq \theta \\ 0 & \text{if } D < \theta \end{cases}, \qquad (5)$$

where D is the membrane displacement, $h_\theta(D)$ is the prediction function (1 = hydrops and 0 = no hydrops), and θ is the diagnostic cutoff. We determined a diagnostic cutoff of 7.36 μm, which maximized Youden's index[33] for training data classification. The sensitivity was 91.7% and the specificity was 85.6% using the running average of five measurements [Fig. 6(d)]. The receiver operating characteristic (ROC) curve, which shows the sensitivity–specificity trade-offs for different diagnostic cutoffs, had an area under curve (AUC) of 0.889 without averaging and 0.955 with averaging [Fig. 5(c)].

Next, we evaluated the trained classifier on the test dataset, which included data from three previously unused mice. This test dataset included 958 automatically measured displacements from 1104 test images and their ground-truth labels. This represented 866 images of cochlea without endolymphatic hydrops and 92 images of cochlea with endolymphatic hydrops, from one control mouse and two noise-exposed mice, respectively. We observed higher automatically measured displacements in images with endolymphatic hydrops compared with in images without endolymphatic hydrops, both without averaging (3.77 ± 4.9 versus 16.22 ± 10.9 μm, mean $\pm$ SD; unpaired t-test, $p < 0.001$) and with averaging of measurements (16.21 ± 7.0 versus 3.77 ± 3.1 μm, mean $\pm$ SD; unpaired t-test, $p < 0.001$) [Fig. 6(a)]. The ROC curve AUC for test data was 0.874 without averaging and 0.961 with averaging [Fig. 6(b)]. The classification of test data showed good sensitivity (0.8261) and specificity (0.8256) without averaging, and higher sensitivity (0.9111) and specificity (0.8773) with averaging such as classification of training data [Figs. 6(d)–6(e)].
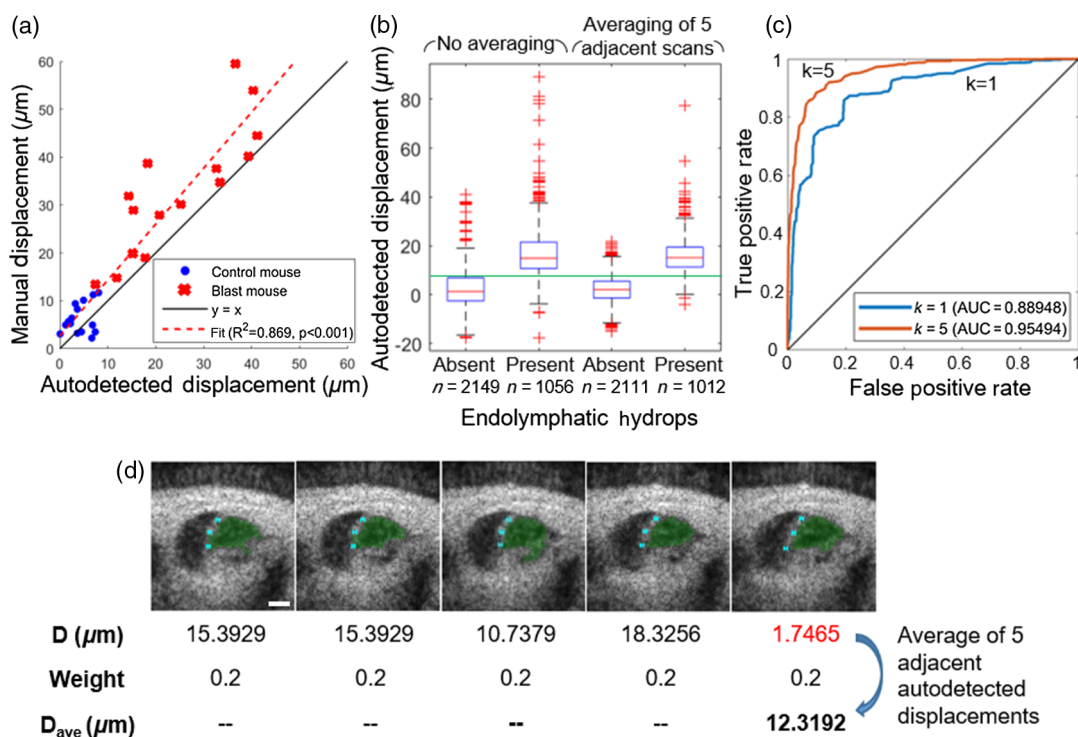
Fig. 5 Automated measurement and classification of training data. (a) Manual versus automated measurements of Reissner's membrane displacement in the same mice described in Fig. 3. Measurements were performed for 30 representative OCT cross sections. (b) Box plots of autodetected displacements in the training dataset, obtained in 13 mice (including the 10 mice described above), with and without averaging of five adjacent measurements. Control ($n = 2149$ measurements) and hydrops ($n = 1056$) without averaging; control ($n = 2111$) and hydrops ($n = 1012$) with averaging. Green line shows the decision threshold of 7.36 μm, which maximized Youden's index for training data classification. Red crosses indicate outliers, defined as values greater than the 75th percentile or less than the 25th percentile by more than 1.5 times the interquartile range. (c) ROC curves showing the sensitivity–specificity trade-offs at different decision thresholds for classifying endolymphatic hydrops (positives) and controls (negatives). $k = 1$, no averaging; $k = 5$, averaging measurements across five adjacent images. (d) Five OCT cross sections, obtained sequentially in time, and their automated displacement measurements. The last (rightmost) image was misclassifed as a control using the nonaveraged measurement (red number) and correctly classified as endolymphatic hydrops using the averaged measurement. The scala media segmentation (green shaded area) and three coordinates for calculating displacement of Reissner's membrane (blue asterisks) identified by the computer program are shown. Scale bar is 100 μm.

Overall, our classifier showed a similar performance between the training and test datasets.

3.5 Error Analysis

Classification of the test dataset resulted in 16 false negatives and 156 false positives. Images corresponding to two of the false negatives and one of the true positives are shown in Fig. 6(c). Each row shows an image at three different steps (shown in different columns) of computer-aided segmentation of Reissner's membrane. From left to right, the columns show the scala media segmentation (green shaded area), Reissner's membrane segmentation (red line), and autodetected coordinates (blue asterisks) for calculating Reissner's membrane displacement.

We observed that misclassification frequently occurred because of errors in segmenting Reissner's membrane. For example, the top row of Fig. 6(c) shows an image in which the upper end point of Reissner's membrane was located too close to the midpoint of the membrane. This resulted in underestimation of the membrane's displacement. (This image also shows an example of the correction to a sharp bend artifact

discussed in step 6(a) of the automated workflow for segmenting Reissner's membrane (Fig. 2). The initial segmentation of Reissner's membrane [Fig. 6(c), red line, middle column] incorrectly includes the attachment area of the tectorial membrane to the spiral limbus; however, step 6(a) removes this portion of the segmentation before determining the end points [Fig. 6(c), blue asterisks, right column].)

Another example of misclassification due to a mistake in segmenting Reissner's membrane is shown in the middle row of Fig. 6(c). In this image, the lower end point of Reissner's membrane was identified up and to the left of its true location. This also resulted in underestimation of Reissner's membrane displacement and caused misclassification of the image as not having endolymphatic hydrops (false negative). Clearly, improving the automated segmentation of Reissner's membrane will be important for increasing the sensitivity and specificity of endolymphatic hydrops classification by this method.

4 Discussion

OCT has provided many benefits for imaging of the inner ear. Mainly, it has provided the ability to perform *in vivo* imaging through the surrounding bone of the otic capsule, whereas
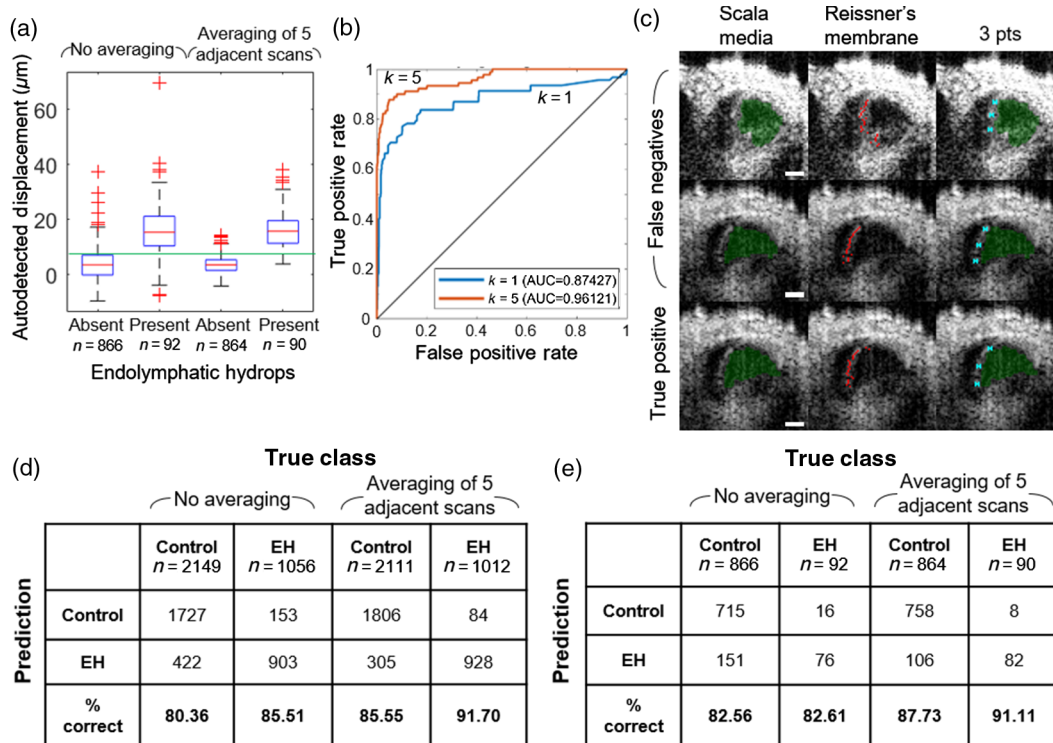
Fig. 6 Classification performance of test data. (a) Automated measurements of Reissner's membrane displacement in the test dataset obtained in three additional mice (not used in the training data). This included one control mouse and two mice with noise-induced endolymphatic hydrops. Green line shows the decision threshold of 7.36 μm. Control ($n = 866$ measurements) and hydrops ($n = 92$) without averaging; control ($n = 864$) and hydrops ($n = 90$) with averaging. (b) ROC curves for the test data, with and without averaging measurements (red line and blue line, respectively). (c) Three OCT cross-sectional images in the test dataset from a mouse with endolymphatic hydrops. Two of the images were misclassified as controls and one was correctly classified as endolymphatic hydrops. Each row shows the same image in a different step of the image analysis workflow. The first column shows the automated segmentation of the scala media (green shaded area); the second column shows the automated segmentation of Reissner's membrane (red line); and the third column shows the three coordinates (3 points; blue asterisks) used to automatically calculate Reissner's membrane displacement. Scale bars are 100 μm. (d) Confusion matrix of training data classification. (e) Confusion matrix of test data classification.

previous anatomic assessment of the cochlea required animal sacrifice with postmortem histological processing. Studies of endolymphatic hydrops have also been hindered by the difficulty of recapitulating the phenomenon of endolymphatic hydrops in model organisms and the absence of objective criteria for evaluating endolymphatic hydrops. Here, we validate Reissner's membrane displacement as an OCT image feature that can be measured manually or automatically and that can be used to classify endolymphatic hydrops with high sensitivity and specificity *in vivo*.

The advantages of this approach are that it is objective and does not need to depend on the user beyond manual cropping of the scala media in the apical cochlear turn. Automated classification overcomes the challenges of subjective grading of endolymphatic hydrops, the standard approach in histopathological, and MRI studies.[14,34] It also overcomes the issue of individual variation of measurements associated with previously described methods that rely on manual segmentation.[21–24]

Another strength of our approach is that it allows estimation of endolymph volume directly from displacement measurements. Previous studies that manually measured scala media area did not describe a model for estimating endolymph volume using those measurements. We also developed our method using

experimental data in live mice, which overcomes challenges associated with fixation in histological cross sections that can distort the appearance of endolymphatic hydrops.[15] Most previous approaches for quantifying endolymphatic hydrops used histological cross sections, though there has been at least one previous study that used OCT imaging.[24]

There are some limitations to our approach. First, the method is semiautomated, requiring manual detection of the apical cochlear turn as a first step. Development of software for automatic detection of the apical cochlear turn would allow this method to become fully automated. Second, this method could analyze only 50% of training images and 87% of test images, indicating that image quality may be a limiting factor. For example, the image quality tended to be lower in the training images compared with the test images (top-left image of Fig. 4 is a training image and the image to its right is a test image). Third, although we found consistent measurements in images acquired at angles between 15 and −15 deg, the influence of imaging angle on measurement of Reissner's membrane displacement may still be important. To account for the potential influence of imaging angle on measurements, a 3-D image of the cochlea could be analyzed rather than single two-dimensional images.

The reproducibility of our method is suggested by the consistency of measurements in cochleae imaged at different positions and depths during experiments, as shown in Fig. 5(d). Although there was some variability between measurements made from different images collected from the same mouse, these were minimal. Moreover, since imaging is done repetitively in practice, averaging can easily be done to reduce the impact of this variability on classification. This was demonstrated in Fig. 5(d). Our method does not involve any random processes, so it produces identical results every time it is run on the same image.

Our method's parameters for performing image processing steps, such as thresholding and morphological operations, may need to be adjusted to analyze datasets acquired by other imaging systems. The parameters do not need to be changed to analyze additional images obtained on our imaging system. However, other imaging setups may produce images at different scales, which would require changing the sizes of structuring elements (parameters for performing morphological operations) to maintain the same physical length scales over which morphological features are assessed. By contrast, the thresholding parameter is automatically chosen for each image using Otsu's method,[32] so this parameter would not need to be adjusted to analyze images with different brightness and contrast levels.

Our method could potentially aid research in endolymphatic hydrops by standardizing measurements and facilitating analysis of large datasets of cochlear OCT images. Standardizing measurements is important to compare the different approaches for inducing endolymphatic hydrops in animal models. This includes surgical obliteration of the endolymphatic duct,[35] genetic mouse models of endolymphatic hydrops,[25] injection with lipopolysaccharide and/or aldosterone,[22] blast exposure,[27] and noise exposure.[19] As more images are collected from different researchers, an automated, objective method will be important for analyzing and comparing these large datasets. The method could also be further developed to be applied to histological images.

Future work will focus on addressing some of the limitations of this method. In addition to the ideas proposed above, one idea is to develop a neural network-based approach. Convolutional neural networks can classify images by automatically learning features from images. This would allow classification of images in which endolymphatic hydrops is visually apparent but difficult to segment using image processing techniques, one of the limitations of the method described here. All input images would be classified, and the neural network may discover additional image features that are important for classifying endolymphatic hydrops. Regardless of the approach, a computer-aided detection method will be important if/when OCT is translated to visualize the human cochlea *in vivo* and could help physicians make reliable detections of endolymphatic hydrops with this technology. In the meantime, our method could potentially aid research in endolymphatic hydrops by standardizing measurements and facilitating analysis of large datasets of cochlear OCT images.

5 Conclusion

We provide, to our knowledge, the first computer-aided method for classifying endolymphatic hydrops in cross-sectional OCT images of the cochlea. Classification with semiautomated measurements yielded a test performance of 91% sensitivity and 88% specificity with averaging of five adjacent measurements.

These findings support the conclusion that computer-aided measurement of Reissner's membrane displacement could aid research in endolymphatic hydrops and, potentially, in translating OCT to point-of-care diagnostics.

References

1. L. M. Sakata et al., "Optical coherence tomography of the retina and optic nerve—a review," *Clin. Exp. Ophthalmol.* **37**, 90–99 (2009).
2. M. L. Gabriele et al., "Optical coherence tomography: history, current status, and laboratory work," *Invest. Ophthalmol. Vis. Sci.* **52**, 2425–2436 (2011).
3. A. M. Zysk et al., "Optical coherence tomography: a review of clinical development from bench to bedside," *J. Biomed. Opt.* **12**, 051403 (2007).
4. H. G. Bezerra et al., "Intracoronary optical coherence tomography: a comprehensive review clinical and research applications," *JACC Cardiovasc. Interventions* **2**, 1035–1046 (2009).
5. L. P. Hariri et al., "Volumetric optical frequency domain imaging of pulmonary pathology with precise correlation to histopathology," *Chest* **143**, 64–74 (2013).
6. M. J. Gora et al., "Tethered capsule endomicroscopy enables less invasive imaging of gastrointestinal tract microstructure," *Nat. Med.* **19**, 238–240 (2013).
7. M. Mogensen et al., "OCT imaging of skin cancer and other dermatological diseases," *J. Biophotonics* **2**, 442–451 (2009).
8. N. H. Cho et al., "In vivo imaging of middle-ear and inner-ear microstructures of a mouse guided by SD-OCT combined with a surgical microscope," *Opt. Express* **22**, 8985–8995 (2014).
9. H. M. Subhash et al., "Volumetric in vivo imaging of intracochlear microstructures in mice by high-speed spectral domain optical coherence tomography," *J. Biomed. Opt.* **15**, 036024 (2010).
10. H. Y. Lee et al., "Noninvasive in vivo imaging reveals differences between tectorial membrane and basilar membrane traveling waves in the mouse cochlea," *Proc. Natl. Acad. Sci. U. S. A.* **112**, 3128–3133 (2015).
11. H. Y. Lee et al., "Two-dimensional cochlear micromechanics measured in vivo demonstrate radial tuning within the mouse organ of corti," *J. Neurosci.* **36**, 8160–8173 (2016).
12. A. Xia et al., "Hair cell force generation does not amplify or tune vibrations within the chicken basilar papilla," *Nat. Commun.* **7**, 1–12 (2016).
13. S. S. Gao et al., "Quantitative imaging of cochlear soft tissues in wild-type and hearing-impaired transgenic mice by spectral domain optical coherence tomography," *Opt. Express* **19**, 15415 (2011).
14. S. Rauch, S. Merchant, and B. Thedinger, "Meniere's syndrome and endolymphatic hydrops double—blind temporal bone study," *Ann. Otol. Rhinol. Laryngol.* **98**, 873–883 (1989).
15. A. N. Salt and S. K. Plontke, "Endolymphatic hydrops: pathophysiology and experimental models," *Otolaryngol. Clin. North Am.* **43**, 971–983 (2010).
16. H. F. Schuknecht, *Pathology of the Ear*, Lea and Febiger, Philadelphia (1993).

17. F. Fiorino et al., "MRI performed after intratympanic gadolinium administration in patients with Ménière's disease: correlation with symptoms and signs," *Eur. Arch. Oto-Rhino-Laryngol.* **268**, 181–187 (2011).

18. H. Fukuoka et al., "Comparison of the diagnostic value of 3 T MRI after intratympanic injection of GBCA, electrocochleography, and the glycerol test in patients with Meniere's disease," *Acta Oto-Laryngol.* **132**, 141–145 (2011).

19. J. Kim et al., "Acute changes in the mouse cochlea after blast injury," in *Abstracts of the Midwinter Research Meeting of the Association for Research in Otolaryngology* (2016).

20. S. F. L. Klis, J. Buijs, and G. F. Smoorenburg, "Quantification of the relation between electrophysiologic and morphologic changes in experimental endolymphatic hydrops," *Ann. Otol. Rhinol. Laryngol.* **99**, 566–570 (1990).

21. T. Takeda et al., "Endolymphatic hydrops induced by chronic administration of vasopressin," *Hear. Res.* **140**, 1–6 (2000).

22. M. Takumida, N. Akagi, and M. Anniko, "A new animal model for Ménière's disease," *Acta Oto-Laryngol.* **128**, 263–271 (2008).

23. A. N. Salt, J. E. DeMott, and R. S. Kimura, "Comparison of endolymph cross-sectional area measured histologically with that measured in vivo with an ionic volume marker," *Ann. Otol. Rhinol. Laryngol.* **104**, 886–894 (1995).

24. A. Kakigi et al., "Evaluation of the internal structure of normal and pathological guinea pig cochleae using optical coherence tomography," *Audiol. Neurotol.* **18**, 335–343 (2013).

25. C. A. Megerian et al., "A mouse model with postnatal endolymphatic hydrops and hearing loss," *Hear. Res.* **237**, 90–105 (2008).

26. S. S. Gao et al., "In vivo vibrometry inside the apex of the mouse cochlea using spectral domain optical coherence tomography," *Biomed. Opt. Express* **4**, 230–240 (2013).

27. S. I. Cho et al., "Mechanisms of hearing loss after blast injury to the ear," *PLoS One* **8**, e67618 (2013).

28. A. Xia et al., "Prestin regulation and function in residual outer hair cells after noise-induced hearing loss," *PLoS One* **8**, e82602 (2013).

29. C. C. Liu et al., "Biophysical mechanisms underlying outer hair cell loss associated with a shortened tectorial membrane," *J. Assoc. Res. Oto-Laryngol.* **12**, 577–594 (2011).

30. J. Lempert et al., "Structure and function of the cochlear aqueduct," *Arch. Otolaryngol.* **55**, 134–145 (1952).

31. L. Vincent, "Morphological grayscale reconstruction in image analysis: applications and efficient algorithms," *IEEE Trans. Image Process.* **2**, 176–201 (1993).

32. N. Otsu, "A threshold selection method from gray-level histograms," *IEEE Trans. Syst. Man Cybern.* **9**, 62–66 (1979).

33. W. J. Youden, "Index for rating diagnostic tests," *Cancer* **3**, 32–35 (1950).

34. K. Baráth et al., "Detection and grading of endolymphatic hydrops in Menière disease using MR imaging," *Am. J. Neuroradiol.* **35**(7), 1387–1392 (2014).

35. C. A. Megerian et al., "Surgical induction of endolymphatic hydrops by obliteration of the endolymphatic duct," *J. Vis. Exp.* (35), e1728 (2010).

George S. Liu is a medical student at Stanford University School of Medicine. He is completing a scholarly concentration in informatics and data-driven medicine, and conducting research funded by the Stanford Medical Scholars Research Program in the Oghalai Lab. His interests involve applying quantitative and machine learning methods to better understand hearing-related disorders. He earned his AB degree in physics with a biophysics certificate from Princeton University.

Jinkyung Kim: Biography is not available.

Brian E. Applegate received his PhD in chemistry from Ohio State University. He won a National Institutes of Health postdoctoral fellowship award to continue his training at Duke University in biomedical engineering. Upon completing his fellowship, he joined the faculty of Texas A&M University where he is currently an associate professor of biomedical engineering. His research interests are broadly to develop innovative biophotonic technologies and apply them to the diagnosis and monitoring of human disease.

John S. Oghalai is a professor at Stanford University. He follows a clinician-scientist pathway with half of his time spent caring for patients and the other half spent performing research. His long-term goals are to better understand the fundamental changes in the inner ear that underlie progressive hearing loss, to develop novel techniques to treat this problem before it worsens, and to determine optimal treatment strategies for patients with severe-to-profound hearing loss.